

# Journal of Materials Chemistry A

Accepted Manuscript



This is an *Accepted Manuscript*, which has been through the Royal Society of Chemistry peer review process and has been accepted for publication.

*Accepted Manuscripts* are published online shortly after acceptance, before technical editing, formatting and proof reading. Using this free service, authors can make their results available to the community, in citable form, before we publish the edited article. We will replace this *Accepted Manuscript* with the edited and formatted *Advance Article* as soon as it is available.

You can find more information about *Accepted Manuscripts* in the [Information for Authors](#).

Please note that technical editing may introduce minor changes to the text and/or graphics, which may alter content. The journal's standard [Terms & Conditions](#) and the [Ethical guidelines](#) still apply. In no event shall the Royal Society of Chemistry be held responsible for any errors or omissions in this *Accepted Manuscript* or any consequences arising from the use of any information it contains.

## Cubic *Pm3n* Supermicroporous Silicas and Aluminosilicates Templated by Short Chain Alkyltrimethylammonium Surfactants

Wen Hua Fu, Sai Jin Wu, Yi Meng Wang \*, Ming Yuan He

*Shanghai Key Lab of Green Chemistry and Chemical Processes, Department of Chemistry, East China Normal University, Shanghai 200062, PR China; Tel: 0086-21-62232251; fax: 0086-21-62232251; E-mail: ymwang@chem.ecnu.edu.cn*

### Abstract

Highly ordered supermicroporous silicas and aluminosilicates with cubic *Pm3n* symmetry were prepared under weakly alkaline condition using alkyltrimethylammonium bromide with short hydrophobic chain and relatively small hydrophilic head as template. As the carbon chain increased from C<sub>10</sub> to C<sub>16</sub>, the packing parameter of surfactants increased and the favored symmetry of silicas shifted from cubic *Pm3n* to hexagonal *p6mm*. Particularly, different mineral acids used to pre-hydrolyze TEOS could tune the silica mesostructures when dodecyltrimethylammonium bromide (C<sub>12</sub>TMAB) was used as template, where sulfuric acid (H<sub>2</sub>SO<sub>4</sub>) led to cubic *Pm3n* symmetry and nitric acid (HNO<sub>3</sub>) resulted in hexagonal *p6mm* symmetry. Under similar conditions, octyltrimethylammonium bromide (C<sub>8</sub>TMAB) templating led to disordered structure. The *Pm3n* symmetry could be well preserved after Al incorporated into the framework and the molar ratio of SiO<sub>2</sub>/Al<sub>2</sub>O<sub>3</sub> in the aluminosilicates reached as low as 25. The pore size of the cubic *Pm3n* silicas and aluminosilicates was in the supermicroporous range. All the silica and aluminosilicate samples exhibited high specific area and large pore volume. For catalytic performance testing, it turned out that compared to zeolite USY-1 and

AlSBA-1 catalyst synthesized in concentrated acid solution, aluminosilicates prepared herein exhibited higher reactivity and pronounced deactivation resistance property in the acetalization of cyclohexanone with pentaerythritol reaction and showed higher yield of 4-*t*-butyl-catechol in the *tert*-butylation of catechol reaction.

**Keywords:** cubic  $Pm3n$ , supermicroporous, alkyltrimethylammonium bromide, packing parameter

## 1. Introduction

Pore size engineering has always been a critical issue in the field of porous materials design.<sup>1</sup> Since crystalline supermicroporous zeolites face diffusion restrict in the large molecule catalysis and conventional ordered mesoporous materials lose shape selectivity in catalysis, supermicroporous materials with pore diameter in the range of 1-2 nm become a candidate for overcoming the above two drawbacks simultaneously.<sup>2</sup> Unlike zeolites and ordered mesoporous materials, which have been highlighted in a lot of reviews,<sup>3-9</sup> much less attention has been paid to non-crystalline ordered supermicroporous materials compared to zeolites and mesoporous materials, in spite of their great importance.<sup>10-30</sup> The reason may lie in that the preparation of supermicroporous materials is always difficult. Generally, synthesis of ordered supermicroporous materials needs the application of templates with short carbon-chain. According to the existence results in the literature, supermicroporous materials are always prepared using surfactants with chain carbon number lower than 12. However, for conventional alkyltrimethylammonium and alkylamine surfactants, the shorter hydrophobic chain results in weaker micellization ability and much higher critical micelle concentration.<sup>31</sup> The inconsistent requirement of

carbon-chain length makes ordered supermicroporous materials quite difficult to obtain. For instance, MCM-41 type silicas template by octyltrimethylammonium or octylamine surfactant are poorly ordered with no more than one diffraction peak exhibiting in the XRD pattern curve.<sup>32-34</sup> Alternatively, double-chain amphiphilic surfactants, also called *Gemini* surfactants, could be applied to the preparation of ordered supermicroporous materials. Thanks to their increased propensity to micelle formation compared to single-chain surfactants with the same alkyl chain length, double-chain surfactants with octyl chains template an ordered silica with  $p6mm$  symmetry.<sup>28</sup> Another alternative is  $\omega$ -hydroxyalkylammonium halide bolaform surfactants employed by Bagshaw *et al.*<sup>25</sup> The micelles formed by  $\omega$ -hydroxy-bolaform surfactant in aqueous solution possess diameters approximately one half of the parent alkyl ammonium halide surfactants and the polar  $\omega$ -hydroxyl function is located near the micelle surface. Supermicroporous silicas with  $L_a$ , SBA-2 ( $P6_3/mmc$ ) and  $Ma$  ( $cm\bar{m}$ ) symmetry have been successfully prepared. Nevertheless, neither the *Gemini* nor Bolaform surfactants can be facily prepared, which limits their applications for the templating of ordered materials. To sum up we would like to devote our efforts to the synthesis of ordered supermicroporous materials by using the conventional alkyltrimethylammonium bromide surfactants with hydrophobic carbon chain length of  $C_{10}$  and  $C_{12}$ . On the other hand, the calculation of the pore size of the so-called supermicroporous materials is still controversial. The most used calculation method is the BJH algorithm, since it always gives narrow pore size distribution curves. However, the BJH method is famous for its underestimating the pore size for the overestimation of the transition pressures caused by the effect of the capillary force on the amount of nitrogen adsorbed.<sup>35</sup> Although more and more researchers have

used geometrical model and non-local density functional theory (NLDFE) method to calculate the pore size,<sup>36,37</sup> the BJH algorithm is still under application and thus results obtained from different works can be compared.

The majority of the supermicroporous materials published in the literature display 2-D hexagonal ( $p6mm$  symmetry) or disordered structures. From the point view of catalysis, three-dimensional pore system offers more accessible pathways for substrates to diffuse in and out compared to disordered or one-dimensional pore system.<sup>38</sup> As a result, the synthesis of ordered supermicroporous materials with 3-D structures is of more significant meaning. Among others,  $Pm3n$  structure with spherical and ellipsoidal cages connected by narrower windows is of particular interest.<sup>39</sup> The cages could be regarded as nanoreactors since their discrete sites provide excellent environment.<sup>40</sup> And the narrower windows offer opportunity for shape selectivity.<sup>41</sup>

The first example of mesoporous silica with  $Pm3n$  structure, SBA-1 was synthesized in concentrated HCl solution using cetyltriethylammonium bromide as template.<sup>42</sup> Afterwards, several mesoporous cubic  $Pm3n$  silicas and aluminosilicates have been prepared. Yet the synthesis of  $Pm3n$  structures always faces the problem of reducing the packing parameter of the surfactant. According to the empirical hypothesis, packing parameter,  $g = V/a_0l$ , of a surfactant should be lower than 1/3 in order to obtain spherical micelles and thus  $Pm3n$  mesophase.<sup>43</sup> As the packing parameter  $g = V/a_0l$ , where  $V$  is the total volume occupied by the hydrophobic tail of a surfactant and the co-solvent (if there is any),  $a_0$  is the area of the interface occupied by every hydrophilic head group, and  $l$  is chain length of the hydrophobic tail,<sup>44</sup> one of the most used way to reduce the  $g$  value is increasing the  $a_0$  value. Keeping this in mind, the general strategies for preparing the

cubic  $Pm3n$  structure can be divided into two categories, one is the usage of surfactants with large head group and the other is enlarging the  $a_0$  value of a certain surfactant by the aid of some auxiliary. The former strategy is clarified by many groups, since the alkyltriethylammonium bromide surfactants are widely used as templates to prepare cubic  $Pm3n$  silicas.<sup>42, 45-52</sup> Other researchers also use alkyltripropylammonium bromide<sup>53</sup> and *Gemini* surfactants<sup>54, 55</sup> as templates. The disadvantage of these methods is always that the surfactants are not commercially available, which making the synthesis more tedious. The latter strategy is achieved by carrying on the synthesis in highly concentrated acid solution<sup>46, 56</sup> or the aid of polyelectrolyte such as Poly(acrylic acid)<sup>57-59</sup> or the aid of co-structure-directing agent (CSDA, aminopropyl-silane is most often used).<sup>60-62</sup> The advantage of this strategy lies in the commercially available alkyltrimethylammonium bromide could be utilized. However, the plethora of acid causes instrument corrosion and contamination problems and the price of Poly(acrylic acid) and CSDA is always pretty high, making this method uneconomical and environmental unfriendly. Therefore the “green” synthesis of cubic  $Pm3n$  silicas using commercial alkyltrimethylammonium surfactants is still under challenge. In fact, Hofmeister anions effect has a great influence on the surfactant self-assembly and the formation of mesoporous solids.<sup>63</sup> Unfortunately, there are so few reports focusing upon the formation of cubic  $Pm3n$  structure combined with the Hofmeister anion effect.<sup>64, 65</sup>

In our previous work, we had successfully prepared a set of supermicroporous silicas and aluminosilicates under alkaline<sup>66</sup> or acidic condition<sup>67</sup> by using dodecyltriethylammonium bromide ( $C_{12}$ TEAB) as template. Herein we report the synthesis of supermicroporous silicas and aluminosilicates with cubic  $Pm3n$  symmetry

using decyltrimethylammonium bromide ( $C_{10}$ TMAB) and dodecyltrimethylammonium bromide ( $C_{12}$ TMAB) as template under weakly alkaline condition. The method report here is facile and fast and the weakly alkaline condition is mild without trouble of serious corrosion. To our best knowledge, it is the first report for the synthesis of cubic  $Pm\bar{3}n$  silicas/aluminosilicates templated by  $C_{10}$ -surfactant or by  $C_{12}$ TMAB surfactant in the absence of any polyelectrolyte or co-structure-directing agent as auxiliary.

The catalytic behavior of the supermicroporous aluminosilicates was tested on acetalization of cyclohexanone with pentaerythritol and *tert*-butylation of catechol with *tert*-butanol. The later one is an important industrial reaction since 4-*tert*-butyl-catechol (4-TBC) and its derivatives are used as raw materials for the synthesis of several polymerization inhibitors, dye developers, pharmaceuticals, and agricultural chemicals.<sup>68</sup> The effect of pore size and structure ordering of the catalysts to the catalytic performance was also discussed.

## 2. Experimental

### 2.1 Synthesis of supermicroporous silicas

In a typical synthesis, the surfactant  $C_{12}$ TMAB or  $C_{10}$ TMAB was dissolved into deionized water followed by acidification of the solution with sulfuric acid. Then TEOS was added and hydrolyzed at room temperature for about 1 h. Under stirring ammonia solution (25 %) was poured into the transparent solution. The final pH value of the mixture was in the range of 8~9. The reaction was carried out at room temperature for another 24 h. After being filtrated, washed by deionized water and dried at 373 K overnight, the solid was calcined at 823 K for 5 h to remove the template. The molar

composition of the mixture was 0.25 C<sub>12</sub>TMAB/0.50 C<sub>10</sub>TMAB : TEOS : 0.11 H<sub>2</sub>SO<sub>4</sub> : 4.5 NH<sub>3</sub> : 500 H<sub>2</sub>O. The silica products were denoted as S-C<sub>12</sub>-H<sub>2</sub>SO<sub>4</sub> and S-C<sub>10</sub>-H<sub>2</sub>SO<sub>4</sub>, where S was short for silica.

In order to investigate the influence of the acids to the product, hydrochloric acid and nitric acid were also used. The concentration of the acids was kept same as using H<sub>2</sub>SO<sub>4</sub>. The products were denoted as S-C<sub>12</sub>-HCl, S-C<sub>10</sub>-HCl, S-C<sub>12</sub>-HNO<sub>3</sub> and S-C<sub>10</sub>-HNO<sub>3</sub>.

## 2.2 Synthesis of supermicroporous aluminosilicates

The synthesis of supermicroporous aluminosilicates was similar to that of silicas. Aluminum sulfate was used as aluminum source and was added into the solution of surfactant before TEOS was added. Sulfuric acid was utilized as acidification reagent. The synthesis was carried out at 273 K for 24 hours. The products were denoted as C<sub>12</sub>-AS-x and C<sub>10</sub>-AS-x, where AS is short for aluminosilicate and x is the molar ratio of SiO<sub>2</sub>/Al<sub>2</sub>O<sub>3</sub> in the initial synthesis gel (for example, C<sub>12</sub>-AS-50 stands for the aluminosilicate sample prepared by C<sub>12</sub>TMAB templating with the initial molar ratio SiO<sub>2</sub>/Al<sub>2</sub>O<sub>3</sub> = 50/1). The calcination procedure was needed to convert the aluminosilicates into H-form.

## 2.3 Characterization

Powder X-ray diffraction (XRD) patterns were recorded on a Rigaku-Ultima diffractometer, with Cu K $\alpha$  radiation at 35 kV and 25 mA. Nitrogen sorption isotherms were measured on a BELSORP-max volumetric adsorption analyzer. The samples were outgassed at 573 K for 6 h before measurement. The BET specific surface area was calculated using adsorption data acquired at a relative pressure (p/p<sub>0</sub>) range of 0.01–0.1

and the total pore volume determined from the amount adsorbed at a relative pressure of about 0.99. The pore size diameters were calculated from the analysis of adsorption branch of the isotherm using the Barrett–Joyner–Halenda (BJH) algorithm.  $^{27}\text{Al}$  solid-state MAS NMR spectra were recorded on a VARIAN VNMRS-400WB spectrometer under a one-pulse condition. The spectra were recorded with a frequency of 104.18 MHz, a spinning rate of 10.0 kHz, and a recycling delay of 4 s.  $\text{KAl}(\text{SO}_4)_2 \cdot 12\text{H}_2\text{O}$  was used as the reference for chemical shift. Inductively coupled plasma atomic emission spectrometry (ICP-AES) was recorded on a Thermo IRIS Intrepid II XSP atomic emission spectrometer after dissolving the samples in HF solution. Temperature-programmed desorption of  $\text{NH}_3$  ( $\text{NH}_3$ -TPD) testing was performed using a TP-5080 chemisorption instrument (Xianquan Co., Ltd, Tianjin, China) with a thermal conductivity detector (TCD). After pretreatment at 550 °C under flowing helium (25 mL/min) for 1 h, each sample (100 mg) was cooled to 100 °C, and then adsorbed to saturation by ammonia for 30 minutes. Ammonia physically adsorbed on the catalyst was removed by flushing the sample with helium (25 mL/min) for 1 h at the adsorption temperature. Thermal desorption of ammonia was carried out in the temperature range of 100–550 °C increasing at a rate of 10 °C/min. Transmission electron microscopy experiments were conducted on TECNAI G2 F30 operating at 300 kV. For the TEM image, the specimens were dispersed in ethanol and placed on holey copper grids.

#### 2.4 Catalytic runs

$\text{C}_{12}\text{-AS-x}$  with  $Pm\bar{3}n$  symmetry was prepared as stated in the above paragraphs.  $\text{C}_{12}\text{-AS-50-HNO}_3$  was obtained following a procedure similar with that of preparation of

C<sub>12</sub>-AS-50, but HNO<sub>3</sub> instead of H<sub>2</sub>SO<sub>4</sub> was used as acidification reagent. Zeolite USY-1 was purchased from Huahua Group Co., Ltd., Wenzhou, China. C<sub>16</sub>-AISBA-1 was prepared by using cetyltriethylammonium bromide, TEOS and aluminum isopropoxide as template, silicon source and aluminum source, respectively. The synthesis procedure was reported by Hartmann *et al.*<sup>69</sup>

#### 2.4.1 Acetalization of cyclohexanone with pentaerythritol

As reported in our previous work,<sup>67</sup> the reaction was carried out under slurry phase reaction conditions using a conventional oil bath attached to a condenser. A typical reaction mixture, in a 10 ml round bottle flask, contained cyclohexanone (20 mmol), pentaerythritol (10 mmol), *n*-decane (10 mmol) and a freshly activated catalyst (50 mg). The reaction was carried out at 120 °C for 2 h. After cooling to room temperature, the flask was washed several times with acetone. All the mixture was collected and separated by centrifugation. The liquid supernatant was analyzed using a Shimadzu GC-2014 gas chromatograph with an Rtx®-Wax capillary column and a flame ionization detector (FID). The conversion was calculated based on cyclohexanone using the internal standard method, where *n*-decane was applied as the internal standard. The formation of diacetals of pentaerythritol was confirmed by GCMS. For recycling runs, the used catalyst was filtered, washed several times with acetone, dried at 100 °C overnight and reused in the next run. The acetalization reaction is illustrated in **Scheme 1A**.

#### 2.4.2 *Tert*-butylation of catechol with *t*-butyl alcohol

*Tert*-butylation of catechol experiments were carried out at atmospheric pressure using a fixed-bed glass reactor (i.d. 6 mm) in the temperature range 125-225 °C. The catalyst was pressed without binder, crushed and sieved to obtain particles with a size of

425~850  $\mu\text{m}$  (20~40 mesh). Typically, 100 mg of catalyst was packed in the middle of the reactor and was activated by flowing  $\text{N}_2$  at 500  $^\circ\text{C}$  for 1 h inside a temperature-controlled furnace. A mixture of catechol and *t*-butyl alcohol with a molar ratio of 1:3 was introduced into the reactor by a peristaltic pump with a catechol based WHSV of about 11.0  $\text{h}^{-1}$ . The liquid products were collected after 1 h using ice-water cooled traps and analyzed by gas chromatography (GC-2014) using a flame ionization detector (FID) furnished with Rtx-Wax 30 m capillary column. The reaction is illustrated in **Scheme 1B**.

### 3. Results and discussion

#### 3.1 Structural properties

The XRD patterns of the silicas templated by  $\text{C}_{12}\text{TMAB}$  are displayed in **Figure 1A**. Three resolved peaks at  $2\theta$  value between 2  $^\circ$  and 4  $^\circ$  are observed in the XRD pattern of the S- $\text{C}_{12}\text{-H}_2\text{SO}_4$  sample (A-a). They are indexed to the (200), (210) and (211) diffraction peaks of the  $Pm\bar{3}n$  symmetry. The peaks at  $2\theta$  value in the range of 4  $^\circ$  to 6  $^\circ$  corresponding to the high-index planes could also be observed. The XRD pattern reveals that the S- $\text{C}_{12}\text{-H}_2\text{SO}_4$  sample possesses the cubic  $Pm\bar{3}n$  structure explicitly. Interestingly, the silicas prepared with HCl and  $\text{HNO}_3$  exhibit different peaks in the XRD patterns. A sharp peak at  $2\theta$  value in the range of 3  $^\circ$  to 4  $^\circ$  and two weak peaks at  $2\theta$  value between 5  $^\circ$  and 7  $^\circ$  are resolved in the XRD pattern of S- $\text{C}_{12}\text{-HNO}_3$  sample. The peaks are indexed to the (100), (110) and (200) diffraction peaks of the hexagonal  $p6mm$  symmetry. The XRD pattern of S- $\text{C}_{12}\text{-HCl}$  is much more complicated and harder to index than the former two. There are several peaks in the  $2\theta$  range of 2  $^\circ$  to 4  $^\circ$ , which cannot be indexed to any

single symmetry. From the XRD pattern of the as-made sample (**Figure S1**), the particular structure can be elucidated more clearly. There are six peaks in the XRD pattern and they are divided into two groups. One group includes three peaks which are indexed to (210), (320) and (422) diffraction peaks of cubic  $Pm3n$  symmetry. The other group consists of the other three peaks and they are indexed to (100), (110) and (200) diffraction peaks of  $p6mm$  symmetry. We believe that the structure obtained with HCl had an intermediate phase between  $p6mm$  symmetry and  $Pm3n$  symmetry. It could be ascribed to an uncompleted phase transformation. Much fewer peaks are observed in the XRD pattern of the calcined sample (A-b), disclosing that the intermediate phase is metastable.

It was an attractive observation that just a small amount of mineral acids used to hydrolyze TEOS could make a great difference to the structure of the final products. It could be explained by the “Hofmeister Anion Effect” on surfactant self-assembly. According to this theory, anions are divided into salting-in (increasing protein solubility) and salting-out (decreasing protein solubility) ones.<sup>63</sup> The Hofmeister order with increasing salting-in potency is  $1/2 \text{SO}_4^{2-} < \text{Cl}^- < \text{NO}_3^-$ . Generally,  $\text{SO}_4^{2-}$  is a typical salting-out anion while  $\text{NO}_3^-$  is a typical salting-in anion. Thanks to their larger hydrated size, salting-out anions are not effective in neutralizing the surfactant charge thus leading to small spherical micelle. That is the case when  $\text{H}_2\text{SO}_4$  was involved in the surfactant solution and thus cubic  $Pm3n$  symmetry could be obtained. As the hydrated size of the ions decreases and the polarizability increases, the salting-in anions shield the electrostatic interactions better, thus allowing the easier formation of rod-like micelles. That is the case when  $\text{HNO}_3$  was used. Rod-like micelles assemble with silicate species

and pack into 2-D hexagonal  $p6mm$  symmetry preferably.  $\text{Cl}^-$  is considered as the boundary between salting-out and salting-in anions. The ability of  $\text{Cl}^-$  to trigger the formation of spherical micelles or rod-like ones is neither too strong nor too weak. Thus it provokes the forming of an intermediate phase. It should be noted here that the hydrolysis of TEOS with small amount of sulfuric acid was prerequisite for the synthesis of cubic  $Pm3n$  silica, in order to maximize the salting-out effect of  $\text{SO}_4^{2-}$  anion. That was completely different with the other synthesis procedures under alkaline condition in the literature, where alkalis were always added initially.

We also prepared cubic  $Pm3n$  silicas using  $\text{C}_{10}\text{TMAB}$  as template for the first time. Regardless of the kind of acids used,  $Pm3n$  symmetry was obtained without exception. **Figure 1B** explicitly shows the characteristic diffraction peaks of the  $Pm3n$  symmetry for all the three silica samples, yet the ordering of these silicas prepared with different acids is in the order of  $\text{H}_2\text{SO}_4 > \text{HCl} > \text{HNO}_3$ . It is the same sequence as the salting-out anion potency.

The  $Pm3n$  structures were proved not only by XRD patterns but also by TEM images. Typical TEM images of calcined S- $\text{C}_{12}$ - $\text{H}_2\text{SO}_4$  sample recorded along the [100], [110] and [111] directions and the corresponding Fourier transform diffractograms (FTs, inserted photographs) are shown in **Figure 2**. The images reveal the uniform channels of 3-D structure and the regular arrays running along a large area, indicating the structure is in highly ordered arrangement. By carefully observation of the FTs, we can confirm the space symmetry of  $Pm3n$ .<sup>60</sup> Indeed, the detailed procedure of the image processing and the electron crystallographic procedure had already been completed by Sakamoto *et al.*<sup>39</sup>

We also tried to synthesize the cubic  $Pm3n$  silicas using alkyltrimethylammonium

bromide surfactants with different hydrophobic chain length as templates and the resultant XRD patterns are displayed in **Figure 3**. As the chain length increased, the silica structures varied from disordered for C<sub>8</sub>TMAB templating to ordered cubic *Pm3n* symmetry for C<sub>10</sub>TMAB and C<sub>12</sub>TMAB templating, and finally to 2-D hexagonal (*p6mm* symmetry) for C<sub>16</sub>TMAB templating. The relationship between the chain length of the surfactants and the structures of the silica products can be interpreted by the empirical equation of packing parameter  $g = V/a_0l$ . According to this, *Pm3n* symmetry is always obtained at a  $g$  value smaller than  $1/3$ ,<sup>43</sup> at which spherical micelles are favored. For C<sub>10</sub>TMAB, the  $a_0$  value occupied by the trimethylammonium head group is relative large, because of the short hydrophobic carbon chain length. That drives the C<sub>10</sub>TMAB surfactants being of  $g$  value smaller than  $1/3$  and being an ideal template to obtain the cubic *Pm3n* silicas. For other alkyltrimethylammonium bromide surfactants, taking account of that the surfactants have the same head group and the longer carbon chain perturbs more intensely, the value of  $V/l$  rises faster than the value of  $a_0$ . As a consequence, the  $g$  value would increase consecutively and the phase region would shift from cubic *Pm3n* symmetry towards *p6mm* symmetry. Consequently there was no chance of obtaining cubic *Pm3n* silica under the circumstance of C<sub>16</sub>TMAB templating. For C<sub>12</sub>TMAB, the  $g$  value may be on the boundary of *ca.*  $1/3$  and taking advantage of Hofmeister salting-out anion (SO<sub>4</sub><sup>2-</sup>) could diminish the  $g$  value thus drive the formation of cubic *Pm3n* symmetry. On the other hand, surfactant with too short carbon chain, such as C<sub>8</sub>TMAB, could hardly template any ordered silicas. The result was in agreement with that in the literature,<sup>32-34</sup> as we stated in the introduction part. The mechanism of forming of the cubic *Pm3n* and hexagonal *p6mm* symmetry in the presence of

alkyltrimethylammonium surfactants is illustrated in **Scheme 2**.

The cubic  $Pm3n$  aluminosilicates were synthesized using  $Al_2SO_4$  as aluminum source. XRD patterns of samples with various molar ratios of  $SiO_2/Al_2O_3$  templated by  $C_{12}TMAB$  and  $C_{10}TMAB$  are presented in **Figure 4**. All the aluminosilicates were highly ordered with  $Pm3n$  symmetry. The  $Pm3n$  symmetry could be well preserved at  $SiO_2/Al_2O_3$  molar ratio as low as 25. The ICP-AES results showed that the molar ratios of  $SiO_2/Al_2O_3$  in the products were almost the same as those in the initial gel, indicating that the utilization of Al source was quite high. Unlike the synthesis of AISBA-1 in concentrated acid solution,<sup>69</sup> where only a very small portion of aluminum source can be incorporated into the product, the weakly alkaline condition herein is beneficial to the incorporation of aluminum. Moreover, the synthesis of the cubic  $Pm3n$  aluminosilicates was free of any alkali metal cations. These materials converted to H-form through the conventional calcination process and then they could be directly used as catalysts without the ammonium exchange procedure.

The coordination state of Al was characterized by the  $^{27}Al$  MAS NMR spectra, as shown in **Figure 5**. All the spectra exhibit two peaks at about 56 ppm and 0 ppm, which are corresponding to the tetrahedrally and octahedrally coordinated Al, respectively. The former peak is much more pronounced than the later one, indicating that majority of Al was incorporated into the framework of the aluminosilicates samples. The existence of extra-framework Al may be ascribed to the usage of  $Al_2(SO_4)_3$  as aluminum source<sup>70</sup> and the rapid precipitation of the aluminosilicates. An interesting finding here was that the ratio of tetrahedrally coordinated Al was higher in aluminosilicates with lower  $SiO_2/Al_2O_3$  molar ratio compared to that in aluminosilicates with higher  $SiO_2/Al_2O_3$ . For

example, the ratio of  $Al_{tetra}/(Al_{tetra} + Al_{octa})$  rose from 0.78 for C<sub>10</sub>-AS-100 to 0.81 C<sub>10</sub>-AS-50 and finally to 0.83 for C<sub>10</sub>-AS-25. We thus obtained highly ordered cubic *Pm3n* aluminosilicates with high Al content and high percentage of framework Al simultaneously.

### 3.2 Textural properties

The textural properties of the silicas and aluminosilicates were characterized by the N<sub>2</sub> physisorption at 77 K and the isotherms are displayed in **Figure 6A**. All the four isotherms present transitional type between typical type I and type IV without any notable capillary condensation or hysteresis loops. The isotherms of C<sub>10</sub>TMAB templated silica and aluminosilicate are ascribed to type I related microporous materials without obvious multilayer adsorption. In **Figure 6B**, the pore size distribution (PSD) curves calculated by the BJH algorithm are presented. It can be observed that the pore diameter of S-C<sub>10</sub>-H<sub>2</sub>SO<sub>4</sub> and C<sub>10</sub>-AS-50 did not exceed 1.3 nm. Given the shape of the isotherms and the PSD curves, it was safe to call the C<sub>10</sub>TMAB templated silicas and aluminosilicates supermicroporous materials. On the other hand, the isotherms of S-C<sub>12</sub>-H<sub>2</sub>SO<sub>4</sub> and C<sub>12</sub>-AS-50 are more or less type IV similar to those of MCM-41 materials. Nevertheless, there is no capillary condensation appearing in the isotherms and only a moderate uptake at a relative pressure lower than  $p/p_0 = 0.2$  is observed. That relative pressure can be regarded as an inflection point, after which the isotherm reaches a plateau. These results were consistent with those of other supermicroporous materials in the literature.<sup>11, 21, 29, 71</sup> The pore size distribution curves in **Figure 6B** exhibits a highest point at pore diameter around 1.7 nm.

The distribution curves of C<sub>12</sub>TMAB templated materials were much narrower than

those of C<sub>10</sub>TMAB templated materials. It may be due to the specific BJH method, since the algorithm is based on the Kelvin equation. It should be kept in mind that capillary condensation would not occur before  $p/p_0 = 0.35$ . This is the reason why the accuracy of the BJH algorithm is doubted, especially for calculating pores smaller than 4 nm. Besides, the BJH model is a macroscopic algorithm regarding fluid-fluid interactions or underestimating wall-fluid interactions in spherical pores. Account for these reasons, Ravikovitch *et al.* developed the non-local density functional theory (NLDFT) to calculate the pore size and they proved that theory was reliable for pore size analysis in cage-like structures, such as SBA-1.<sup>37</sup> We thus applied the NLDFT method for the pore size calculation and the corresponding PSD curves are presented in **Figure 6C**. According to the NLDFT method, the pore size of C<sub>12</sub>TMAB templated silica and aluminosilicate exceeded 2 nm and that of C<sub>10</sub>TMAB templated materials was on the lower boundary of mesopore. The curves are no longer narrow, even for the C<sub>12</sub>TMAB templated materials. In some cases, the curves exhibit more than one peak, as shown by curve **a** and **c**. We argued that the NLDFT model could be not that suitable for the silicas and aluminosilicates prepared herein. In fact, there wasn't a widely accepted model to calculate the pore diameter of supermicroporous materials. As stated in the introduction part, we could compare our physisorption results with those in other publications. The pore diameters calculated with the BJH model in this paper were very close to those of supermicroporous materials reported by other groups.<sup>11, 17, 18, 29, 72</sup> More reliable results could be found in other articles, since researchers combined NLDFT algorithm and TEM method to calculate the pore size of supermicroporous silicas with *p6mm* symmetry.<sup>16, 21,</sup>  
<sup>23</sup> We ensured that the shape of the isotherms of C<sub>10</sub>TMAB templated silica and

aluminosilicate were similar to, or even more type-I like than those reported in their papers. Consequently, being controversial, we still applied the BJH method to estimate the pore size of the silica and aluminosilicate materials and insisted to term them supermicroporous materials, particularly for the C<sub>10</sub>TMAB templated ones.

The textural properties of the silica and aluminosilicate materials are listed in **Table 1**. High specific area and pore volume was obtained for all the four samples. Silica and aluminosilicate prepared using longer C<sub>12</sub>TMAB template possessed higher specific area, higher pore volume and larger pore diameter than those prepared using C<sub>10</sub>TMAB as template. And the specific area, pore volume and pore size enlarged slightly because of the incorporation of Al into the siliceous framework.

### 3.3 Catalytic properties

The results of acetalization of cyclohexanone with pentaerythritol over different catalysts are listed in **Table 2**. The conversions of cyclohexanone over all the aluminosilicates prepared in this study were almost the same and exceeded 40 %, except that over C<sub>12</sub>-AS-100 with low content of Al. For USY-1 with micropores, the conversion was much lower. Zeolites are famous for their strong acidity, but they are not efficient in this reaction, since the bulky product molecule could be occluded in the pores. The conversion over C<sub>16</sub>-AISBA-1 with large pore was lower than C<sub>12</sub>-AS-x catalyst with similar SiO<sub>2</sub>/Al<sub>2</sub>O<sub>3</sub> molar ratio. The acidity of the two kinds of aluminosilicates was similar, as shown by the NH<sub>3</sub>-TPD profiles (**Figure S3**). As the introduction of Al into the framework, the ordering of C<sub>16</sub>-AISBA-1 was much poorer than C<sub>12</sub>-AS-x and that was probably responsible for the low conversion of cyclohexanone. Recyclability studies of the C<sub>16</sub>-AISBA-1(56), C<sub>12</sub>-AS-50 and USY-1 catalysts were investigated and the results

are disclosed by **Figure 7**. For C<sub>12</sub>-AS-50 the conversion of cyclohexanone did not decrease during the recycled catalysis, showing that catalyst was of pronounced deactivation resistance. For USY-1 and C<sub>16</sub>-AISBA-1(56), the conversion depressed remarkably and decreased to lower than 5 % at the 2<sup>nd</sup> or 3<sup>rd</sup> cycle. It was obvious that the aluminosilicates prepared in this study showed not only higher activities but also stronger deactivation resistant ability.

The alkylation of catechol with *tert*-butyl alcohol (TBA) was used as another probe reaction to explore the catalytic performance of aluminosilicate catalysts. In general, the main products were 4-*t*-butyl-catechol (4-TBC), 3-*t*-butyl-catechol (3-TBC) and 3,5-di-*t*-butyl-catechol (3,5-DTBC) as illustrated in **Scheme 1B**. The XRD patterns of C<sub>12</sub>-AS-50-HNO<sub>3</sub> and C<sub>16</sub>-AISBA-1 are displayed in **Figure S2**. The effects of the reaction temperature in the *t*-butylation of catechol with TBA using different catalysts in 125-225 °C range are summarized in **Table 3**. In all cases, 4-TBC was the predominant product. On account of the electrophilic nature of the alkylation reaction over acidic catalysts, substitution at the *para*-position of catechol is favored.<sup>68</sup>

The conversion of catechol over USY-1 and C<sub>12</sub>-AS-50 increased as the reaction temperature rose from 125 °C to 175 °C. A further increase in the reaction temperature led to considerable decrease in conversion. The reason may lie in more pronounced dealkylation effect and the diminishing availability of TBA as it underwent side reactions such as oligomerization or aromatization at higher reaction temperature, which had been observed in the alkylation of aromatics published in other articles.<sup>73, 74</sup> The maximum conversion of catechol was obtained at 175 °C over USY-1 and C<sub>12</sub>-AS-50 and the maximum was 60.9 % and 74.3 %, respectively. The variation of catechol conversion

over  $C_{12}$ -AS-50- $HNO_3$  and  $C_{16}$ -AISBA-1 catalysts at different reaction temperatures was similar to that of the former two catalysts, yet the maximum conversion was obtained at lower temperature, 150 °C. The selectivity for 4-TBC continuously elevated with the increasing of the reaction temperature, while the selectivity of dialkylated product 3,5-DTBC varied totally on the opposite direction. The selectivity of 3-TBC was highest at 125 °C and just changed slightly at higher temperature. The variation of yield of 4-TBC was similar to that of catechol conversion.

Among the four catalysts,  $C_{12}$ -AS-50 with ordered supermicroporous and three-dimensional pore system gave the highest catechol conversion (74.3 %) and yield of 4-TBC (63.6 %). From the point view of maximizing the yield of 4-TBC, the best catalyst was  $C_{12}$ -AS-50 and the best reaction temperature was 175 °C. The selectivity of 4-TBC was highest over USY-1. Even at low temperature, the selectivity of 4-TBC was no lower than 88.0 %. The reason probably lay in the most restricted pore system of USY-1 among all the four catalysts. Generally speaking, shape selectivity occurs in pores with smaller diameter. The pore size of zeolite USY-1 is not large enough to accommodate the bulky molecule 3,5-DTBC, so the selectivity for 3,5-DTBC over USY-1 was low. Although the limited diffusion in the pores of USY-1 raised the selectivity of 4-TBC in the products, the activity of the catalyst was depressed, resulting a lower catechol conversion. Consequently, although the selectivity of 4-TBC over USY-1 was higher than that over  $C_{12}$ -AS-50, the maximum yield of 4-TBC was about 11.5 % lower (56.3 % versus 63.6 %) over zeolite USY-1.

Unlike  $C_{12}$ -AS-50 with  $Pm3n$  symmetry,  $C_{12}$ -AS-50- $HNO_3$  was of one-dimensional pore structure with  $p6mm$  symmetry. As stated in the introduction part, diffusion restrain

is more pronounced in one-dimensional pores than in three-dimensional pores. As a result, the catechol conversion and the yield of 4-TBC over  $C_{12}$ -AS-50- $HNO_3$  were much lower than those over  $C_{12}$ -AS-50. The selectivity of 4-TBC over  $C_{12}$ -AS-50- $HNO_3$  was slightly lower than that over  $C_{12}$ -AS-50. It should be ascribed to the longer pathway or longer diffusion period over the former catalyst and the presence of isomerization of 4-TBC to 3-TBC.

The *t*-butylation reaction carried on over  $C_{16}$ -AISBA-1 with absolutely unrestricted pore structure helped to increase neither the catechol conversion nor the yield of 4-TBC. On the contrary, the catechol conversion and the yield of 4-TBC were both lower than those in the case of  $C_{12}$ -AS-50 catalysis. The reason may lie in that the  $C_{16}$ -AISBA-1 sample was prepared in concentrated acid solution (section 2.4), which led to poor utilization of Al source and severely perturbed structure ordering. XRD pattern of  $C_{16}$ -AISBA-1 indicates that the sample is much less ordered than  $C_{12}$ -AS-50 sample (supplementary information, **Figure S2**).

In summary, thanks to the less limited pore system and well-ordered structure, the supermicroporous aluminosilicates with *Pm3n* symmetry was the most suitable for the alkylation of catechol with *tert*-butyl alcohol. The catechol conversion and the yield of 4-TBC were as high as 74.3 % and 63.6 %, respectively.

#### 4. Conclusion

In summary, highly ordered supermicroporous silicas and aluminosilicates with *Pm3n* symmetry were obtained by using dodecyltrimethylammonium bromide and decyltrimethylammonium bromide as templates. The effect of mineral acid for

pre-hydrolyzing TEOS and the hydrophobic carbon chain length of the surfactants on the products structures were investigated and interpreted by the “Hofmeister Anion Effect” and the packing parameter of surfactant, respectively. The supermicroporosity was discussed by characterization with N<sub>2</sub> physisorption. The incorporation of Al into the framework slightly perturbed the ordering and ordered aluminosilicates with low SiO<sub>2</sub>/Al<sub>2</sub>O<sub>3</sub> molar ratio (*ca.* 25) could be facily obtained. The catalytic performance of the *Pm3n* aluminosilicates was investigated by acetalization of cyclohexanone and *tert*-butylation of catechol reaction and catalysts prepared here exhibited superior performance to USY-1 zeolite and C<sub>16</sub>-AISBA-1 catalysts.

### Acknowledgements

This work is supported by National Key Technology R&D Program (No. 2012BAE05B02) and National Science Foundation of China (20890122). And Prof. Wang thanks for the Fundamental Research Funds for the Central Universities and the Program for New Century Excellent Talents in University (NCET-11-0145), Ministry of Education of China.

### References

1. A. Sayari, M. Kruk, M. Jaroniec and I. L. Moudrakovski, *Adv. Mater.*, 1998, **10**, 1376-1379.
2. M. M. Dubinin, *J. Colloid Interface Sci.*, 1974, **46**, 351-356.
3. A. Corma, *Chem. Rev.*, 1997, **97**, 2373-2420.
4. J. Y. Ying, C. P. Mehnert and M. S. Wong, *Angew. Chem. Int. Ed.*, 1999, **38**, 56-77.
5. C. S. Cundy and P. A. Cox, *Chem. Rev.*, 2003, **103**, 663-702.

6. Y. Wan and Zhao, *Chem. Rev.*, 2007, **107**, 2821-2860.
7. W. Vermeiren and J. P. Gilson, *Top. Catal.*, 2009, **52**, 1131-1161.
8. R. Chal, C. Gérardin, M. Bulut and S. van Donk, *ChemCatChem*, 2011, **3**, 67-81.
9. C. Perego and R. Millini, *Chem. Soc. Rev.*, 2013, **42**, 3956-3976.
10. X. Song Zhao, G. Q. Lu and X. Hu, *Chem. Commun.*, 1999, 1391-1392.
11. Y. Di, X. Meng, L. Wang, S. Li and F.-S. Xiao, *Langmuir*, 2006, **22**, 3068-3072.
12. B. L. Newalkar, H. Katsuki and S. Komarneni, *Micro. Meso. Mater.*, 2004, **73**, 161-170.
13. Y. Zhou and M. Antonietti, *Chem. Mater.*, 2004, **16**, 544-550.
14. M. Polverejan, Y. Liu and T. J. Pinnavaia, *Chem. Mater.*, 2002, **14**, 2283-2288.
15. L. Huerta, F. Romero-Sarria, O. Marie, C. Guillem, A. Beltrán, J. Latorre, D. Beltrán and P. Amorós, *Eur. J. Inorg. Chem.*, 2006, **2006**, 3147-3151.
16. N. Alam and R. Mokaya, *Micro. Meso. Mater.*, 2011, **143**, 104-114.
17. M. Kato, T. Shigeno, T. Kimura and K. Kuroda, *Chem. Mater.*, 2005, **17**, 6416-6421.
18. M. Kruk, T. Asefa, M. Jaroniec and G. A. Ozin, *J. Am. Chem. Soc.*, 2002, **124**, 6383-6392.
19. E. Bastardo-Gonzalez, R. Mokaya and W. Jones, *Chem. Commun.*, 2001, 1016-1017.
20. C. Rodríguez-Abreu, C. Aubery-Torres, C. Solans, A. López-Quintela and G. J. T. Tiddy, *ACS Applied Materials & Interfaces*, 2011, **3**, 4133-4141.
21. A. K. L. Yuen, F. Heinroth, A. J. Ward, A. F. Masters and T. Maschmeyer, *Micro. Meso. Mater.*, 2012, **148**, 62-72.
22. Y. Yamada and K. Yano, *Micro. Meso. Mater.*, 2006, **93**, 190-198.
23. K. Yano and Y. Fukushima, *J. Mater. Chem.*, 2003, **13**, 2577-2581.
24. M. D. McNall, J. Scott, L. Mercier and P. J. Kooyman, *Chem. Commun.*, 2001, 2282-2283.
25. S. A. Bagshaw and A. R. Hayman, *Chem. Commun.*, 2000, 533-534.
26. D. Zhao, Q. Huo, J. Feng, J. Kim, Y. Han and G. D. Stucky, *Chem. Mater.*, 1999, **11**, 2668-2672.
27. T. Sun, M. S. Wong and J. Y. Ying, *Chem. Commun.*, 2000, 2057-2058.

28. R. Ryoo, I.-S. Park, S. Jun, C. W. Lee, M. Kruk and M. Jaroniec, *J. Am. Chem. Soc.*, 2001, **123**, 1650-1657.
29. R. Wang, S. Han, W. Hou, L. Sun, J. Zhao and Y. Wang, *J. Phys. Chem. C*, 2007, **111**, 10955-10958.
30. Y.-S. Lin, H.-P. Lin and C.-Y. Mou, *Micro. Meso. Mater.*, 2004, **76**, 203-208.
31. K. Holmberg, B. Jönsson, B. Kronberg and B. Lindman, in *Surfactants and Polymers in Aqueous Solution*, John Wiley & Sons, Ltd, 2003, pp. 39-66.
32. P. T. Tanev and T. J. Pinnavaia, *Chem. Mater.*, 1996, **8**, 2068-2079.
33. J. S. Beck, J. C. Vartuli, G. J. Kennedy, C. T. Kresge, W. J. Roth and S. E. Schramm, *Chem. Mater.*, 1994, **6**, 1816-1821.
34. C. G. Sonwane, S. K. Bhatia and N. Calos, *Ind. Eng. Chem. Res.*, 1998, **37**, 2271-2283.
35. M. Kruk and M. Jaroniec, *Chem. Mater.*, 2001, **13**, 3169-3183.
36. P. I. Ravikovitch, G. L. Haller and A. V. Neimark, *Adv. Colloid Interface Sci.*, 1998, **76**, 203-226.
37. P. I. Ravikovitch and A. V. Neimark, *Langmuir*, 2002, **18**, 1550-1560.
38. P. Srinivasu, S. Alam, V. V. Balasubramanian, S. Velmathi, D. P. Sawant, W. Böhlmann, S. P. Mirajkar, K. Ariga, S. B. Halligudi and A. Vinu, *Adv. Funct. Mater.*, 2008, **18**, 640-651.
39. Y. Sakamoto, M. Kaneda, O. Terasaki, D. Y. Zhao, J. M. Kim, G. Stucky, H. J. Shin and R. Ryoo, *Nature*, 2000, **408**, 449-453.
40. Q. Yang, D. Han, H. Yang and C. Li, *Chemistry – An Asian Journal*, 2008, **3**, 1214-1229.
41. S. M. Csicsery, *Zeolites*, 1984, **4**, 202-213.
42. Q. Huo, D. I. Margolese, U. Ciesla, P. Feng, T. E. Gier, P. Sieger, R. Leon, P. M. Petroff, F. Schuth and G. D. Stucky, *Nature*, 1994, **368**, 317-321.
43. Q. Huo, D. I. Margolese and G. D. Stucky, *Chem. Mater.*, 1996, **8**, 1147-1160.
44. J. N. Israelachvili, D. J. Mitchell and B. W. Ninham, *J. Chem. Soc., Faraday Trans. 2*, 1976, **72**, 1525-1568.
45. Q. Huo, D. I. Margolese, U. Ciesla, D. G. Demuth, P. Feng, T. E. Gier, P. Sieger, A. Firouzi and B. F. Chmelka, *Chem. Mater.*, 1994, **6**, 1176-1191.

46. M. J. Kim and R. Ryoo, *Chem. Mater.*, 1999, **11**, 487-491.
47. S. Che, S. Kamiya, O. Terasaki and T. Tatsumi, *J. Am. Chem. Soc.*, 2001, **123**, 12089-12090.
48. S. Che, Y. Sakamoto, O. Terasaki and T. Tatsumi, *Chem. Mater.*, 2001, **13**, 2237-2239.
49. A. Vinu, V. Murugesan and M. Hartmann, *Chem. Mater.*, 2003, **15**, 1385-1393.
50. H.-M. Kao, C.-C. Cheng, C.-C. Ting and L.-Y. Hwang, *J. Mater. Chem.*, 2005, **15**, 2989-2992.
51. H.-M. Kao, C.-C. Ting, A. S. T. Chiang, C.-C. Teng and C.-H. Chen, *Chem. Commun.*, 2005, 1058-1060.
52. M.-C. Liu, C.-S. Chang, J. C. C. Chan, H.-S. Sheu and S. Cheng, *Micro. Meso. Mater.*, 2009, **121**, 41-51.
53. H.-M. Kao, Y.-W. Liao and C.-C. Ting, *Micro. Meso. Mater.*, 2007, **98**, 80-88.
54. H. I. Lee, C. Pak, S. H. Yi, J. K. Shon, S. S. Kim, B. G. So, H. Chang, J. E. Yie, Y.-U. Kwon and J. M. Kim, *J. Mater. Chem.*, 2005, **15**, 4711-4717.
55. A. E. Garcia-Bennett, S. Williamson, P. A. Wright and I. J. Shannon, *J. Mater. Chem.*, 2002, **12**, 3533-3540.
56. C.-C. Ting, H.-Y. Wu, A. Palani, A. S. T. Chiang and H.-M. Kao, *Micro. Meso. Mater.*, 2008, **116**, 323-329.
57. N. Li, J.-G. Wang, H.-J. Zhou, P.-C. Sun and T.-H. Chen, *Chem. Mater.*, 2011, **23**, 4241-4249.
58. N. Li, J.-G. Wang, J.-X. Xu, J.-Y. Liu, H.-J. Zhou, P.-C. Sun and T.-H. Chen, *Nanoscale*, 2012, **4**, 2150-2156.
59. C. C. Pantazis and P. J. Pomonis, *Chem. Mater.*, 2003, **15**, 2299-2300.
60. R. Atluri, Y. Sakamoto and A. E. Garcia-Bennett, *Langmuir*, 2009, **25**, 3189-3195.
61. S. Che, A. E. Garcia-Bennett, T. Yokoi, K. Sakamoto, H. Kunieda, O. Terasaki and T. Tatsumi, *Nat. Mater.*, 2003, **2**, 801-805.
62. T. Suteewong, H. Sai, R. Cohen, S. Wang, M. Bradbury, B. Baird, S. M. Gruner and U. Wiesner, *J. Am. Chem. Soc.*, 2011, **133**, 172-175.
63. E. Leontidis, *Curr. Opin. Colloid Interface Sci.*, 2002, **7**, 81-91.
64. S. Che, S. Lim, M. Kaneda, H. Yoshitake, O. Terasaki and T. Tatsumi, *J. Am.*

- Chem. Soc.*, 2002, **124**, 13962-13963.
65. S. Che, H. Li, S. Lim, Y. Sakamoto, O. Terasaki and T. Tatsumi, *Chem. Mater.*, 2005, **17**, 4103-4113.
66. W. Hua Fu, Y. Meng Wang and M.-Y. He, *Mater. Lett.*, 2013, **109**, 127-129.
67. W. H. Fu, Y. M. Wang and M. Y. He, *RSC Advances*, 2013, **3**, 18519-18528.
68. J. W. Yoo, C. W. Lee, S.-E. Park and J. Ko, *Applied Catalysis A: General*, 1999, **187**, 225-232.
69. M. Hartmann, A. Vinu, S. P. Elangovan, V. Murugesan and W. Bohlmann, *Chem. Commun.*, 2002, 1238-1239.
70. H. Kosslick, G. Lischke, B. Parlitz, W. Storek and R. Fricke, *Applied Catalysis A: General*, 1999, **184**, 49-60.
71. S. A. Bagshaw and A. R. Hayman, *Adv. Mater.*, 2001, **13**, 1011-1013.
72. X. Guo, N. Xue, S. Liu, X. Guo, W. Ding and W. Hou, *Micro. Meso. Mater.*, 2007, **106**, 246-255.
73. K. Zhang, H. Zhang, G. Xu, S. Xiang, D. Xu, S. Liu and H. Li, *Applied Catalysis A: General*, 2001, **207**, 183-190.
74. A. Vinu, T. Krithiga, V. V. Balasubramanian, A. Asthana, P. Srinivasu, T. Mori, K. Ariga, G. Ramanath and P. G. Ganesan, *J. Phys. Chem. B*, 2006, **110**, 11924-11931.

**Scheme, Figure Captions and Tables**

**Figure 1** XRD patterns of calcined silicas templated by C<sub>12</sub>TMAB (A) and C<sub>10</sub>TMAB (B): (A-a) S-C<sub>12</sub>-H<sub>2</sub>SO<sub>4</sub>, (A-b) S-C<sub>12</sub>-HCl, (A-c) S-C<sub>12</sub>-HNO<sub>3</sub>, (B-a) S-C<sub>10</sub>-H<sub>2</sub>SO<sub>4</sub>, (B-b) S-C<sub>10</sub>-HCl and (B-c) S-C<sub>10</sub>-HNO<sub>3</sub>.

**Figure 2** Transmission electron micrograph images and the corresponding Fourier transform diffractograms (inserted photographs) of S-C<sub>12</sub>-H<sub>2</sub>SO<sub>4</sub> viewed along different zone axes: (A) [100], (B) [110] and (C) [111].

**Figure 3** XRD patterns of as-made silicas templated by alkyltrimethylammonium bromide surfactants with different chain length: (a) C<sub>8</sub>TMAB, (b) C<sub>10</sub>TMAB, (c) C<sub>12</sub>TMAB, and (d) C<sub>16</sub>TMAB.

**Figure 4** XRD patterns of calcined aluminosilicates templated by C<sub>12</sub>TMAB (A) and C<sub>10</sub>TMAB (B): (A-a) C<sub>12</sub>-AS-100, (A-b) C<sub>12</sub>-AS-75, (A-c) C<sub>12</sub>-AS-50, (A-d) C<sub>12</sub>-AS-25, (B-a) C<sub>10</sub>-AS-100, (B-b) C<sub>10</sub>-AS-75, (B-c) C<sub>10</sub>-AS-50 and (B-d) C<sub>10</sub>-AS-25.

**Figure 5** <sup>27</sup>Al MAS NMR spectra of aluminosilicates: (a) C<sub>12</sub>-AS-100, (b) C<sub>12</sub>-AS-50, (c) C<sub>12</sub>-AS-25, (d) C<sub>10</sub>-AS-100, (e) C<sub>10</sub>-AS-50 and (f) C<sub>10</sub>-AS-25.

**Figure 6** N<sub>2</sub> adsorption-desorption isotherms (A) and pore size distribution calculated by BJH model (B) and NLDFT model (C) of silicas and aluminosilicates: (a) S-C<sub>12</sub>-H<sub>2</sub>SO<sub>4</sub>, (b) C<sub>12</sub>-AS-50, (c) S-C<sub>10</sub>-H<sub>2</sub>SO<sub>4</sub> and (d) C<sub>10</sub>-AS-50.

**Figure 7** Recyclability studies of the various catalysts in the acetalization of cyclohexanone with pentaerythritol.

**Scheme 1A** Acetalization of cyclohexanone with pentaerythritol.

**Scheme 1B** Illustration of alkylation of catechol with *tert*-butyl alcohol.

**Scheme 2** Illustration of the forming of cubic  $Pm\bar{3}n$  and hexagonal  $p6mm$  structures templated by alkyltrimethylammonium bromide surfactants.

**Table 1** Textural properties of silicas and aluminosilicates templated by  $C_{12}$ TMAB and  $C_{10}$ TMAB.

**Table 2** Results of acetalization of cyclohexanone with pentaerythritol over different catalysts.

**Table 3** Results of *tert*-butylation of catechol over different catalysts at various reaction temperatures.

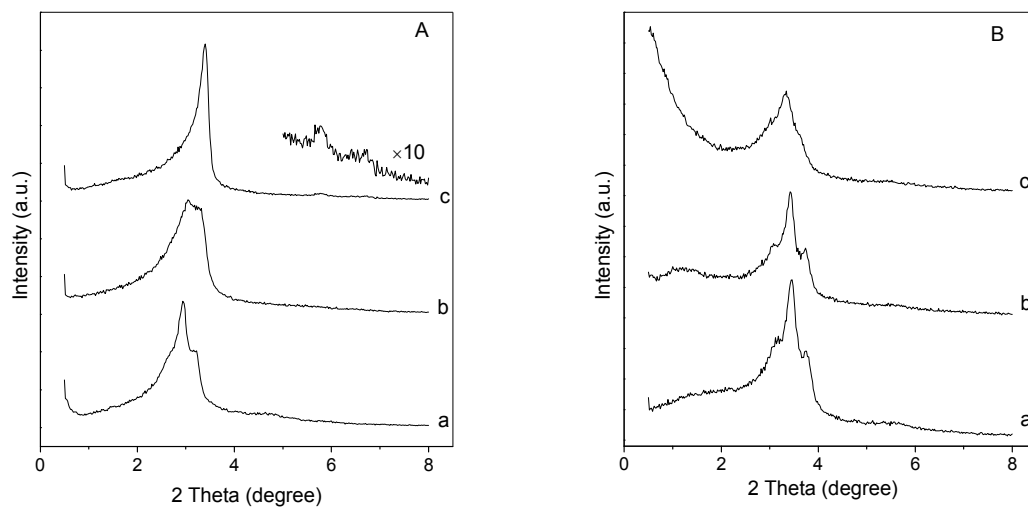


**Figure 1** XRD patterns of calcined silicas templated by C<sub>12</sub>TMAB (A) and C<sub>10</sub>TMAB (B): (A-a) S-C<sub>12</sub>-H<sub>2</sub>SO<sub>4</sub>, (A-b) S-C<sub>12</sub>-HCl, (A-c) S-C<sub>12</sub>-HNO<sub>3</sub>, (B-a) S-C<sub>10</sub>-H<sub>2</sub>SO<sub>4</sub>, (B-b) S-C<sub>10</sub>-HCl and (B-c) S-C<sub>10</sub>-HNO<sub>3</sub>.

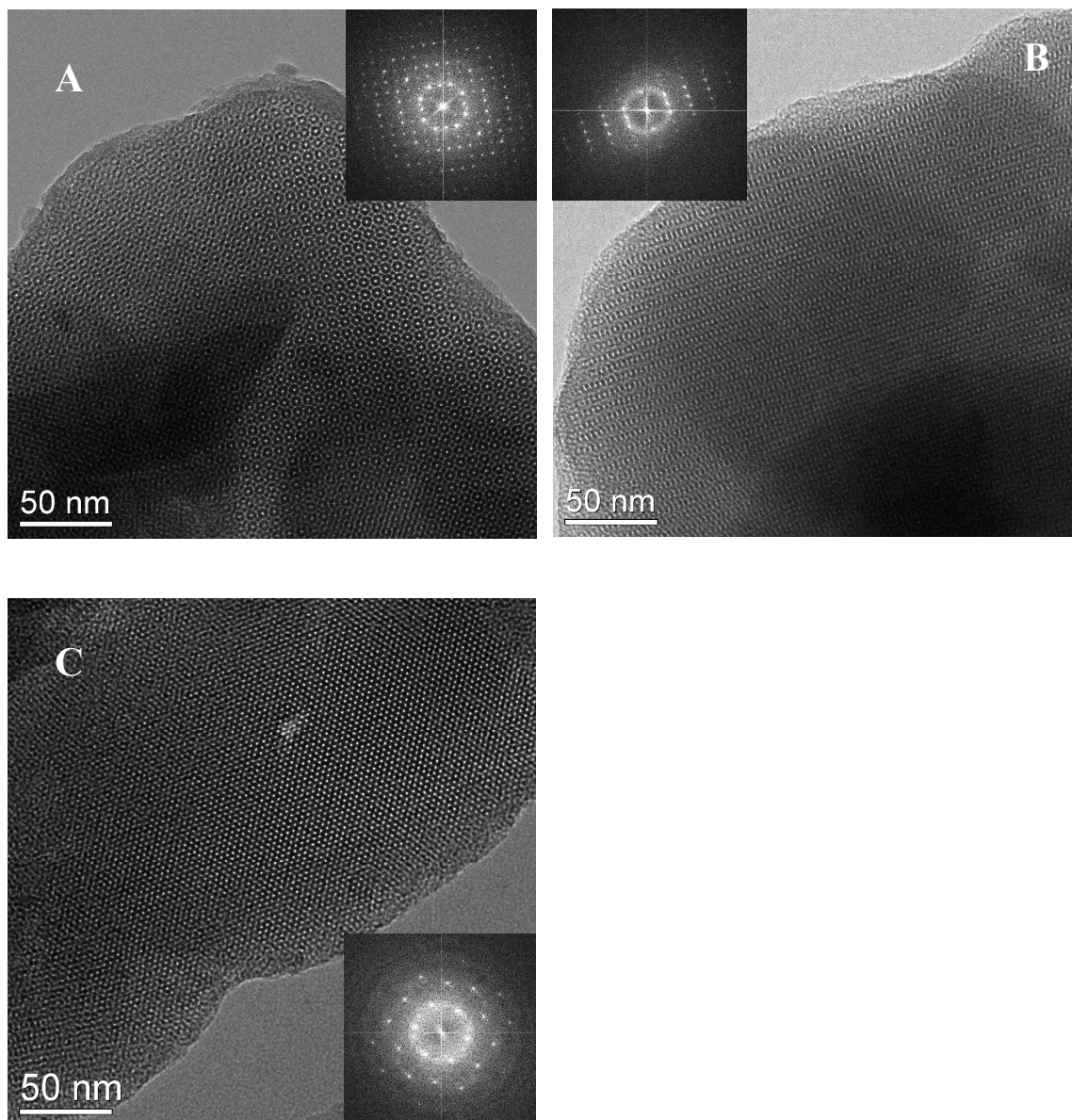


**Figure 2** Transmission electron micrograph images and the corresponding Fourier transform diffractograms (inserted photographs) of S-C<sub>12</sub>-H<sub>2</sub>SO<sub>4</sub> viewed along different zone axes: (A) [100], (B) [110] and (C) [111].

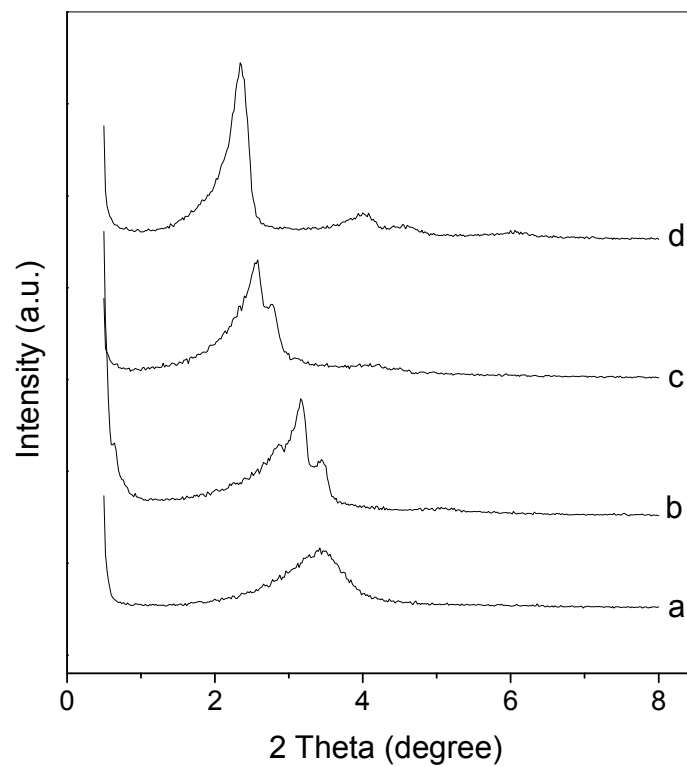


**Figure 3** XRD patterns of as-made silicas templated by alkyltrimethylammonium bromide surfactants with different chain length: (a) C<sub>8</sub>TMAB, (b) C<sub>10</sub>TMAB, (c) C<sub>12</sub>TMAB, and (d) C<sub>16</sub>TMAB.

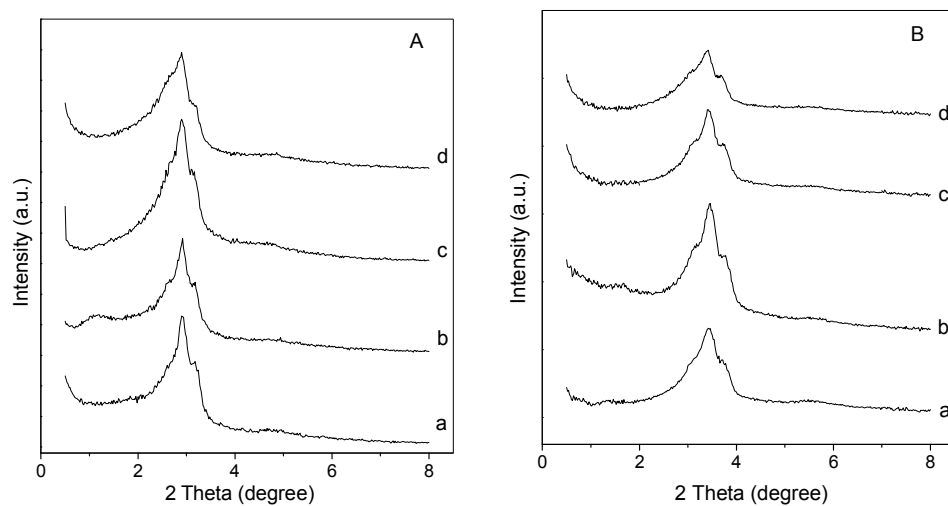


**Figure 4** XRD patterns of calcined aluminosilicates templated by  $C_{12}$ TMAB (A) and  $C_{10}$ TMAB (B): (A-a)  $C_{12}$ -AS-100, (A-b)  $C_{12}$ -AS-75, (A-c)  $C_{12}$ -AS-50, (A-d)  $C_{12}$ -AS-25, (B-a)  $C_{10}$ -AS-100, (B-b)  $C_{10}$ -AS-75, (B-c)  $C_{10}$ -AS-50 and (B-d)  $C_{10}$ -AS-25.

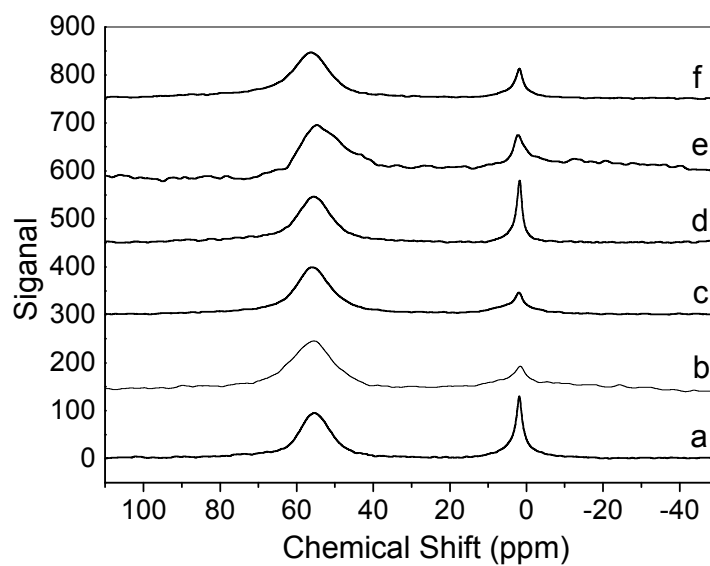


**Figure 5**  $^{27}\text{Al}$  MAS NMR spectra of aluminosilicates: (a)  $\text{C}_{12}\text{-AS-100}$ , (b)  $\text{C}_{12}\text{-AS-50}$ , (c)  $\text{C}_{12}\text{-AS-25}$ , (d)  $\text{C}_{10}\text{-AS-100}$ , (e)  $\text{C}_{10}\text{-AS-50}$  and (f)  $\text{C}_{10}\text{-AS-25}$ .

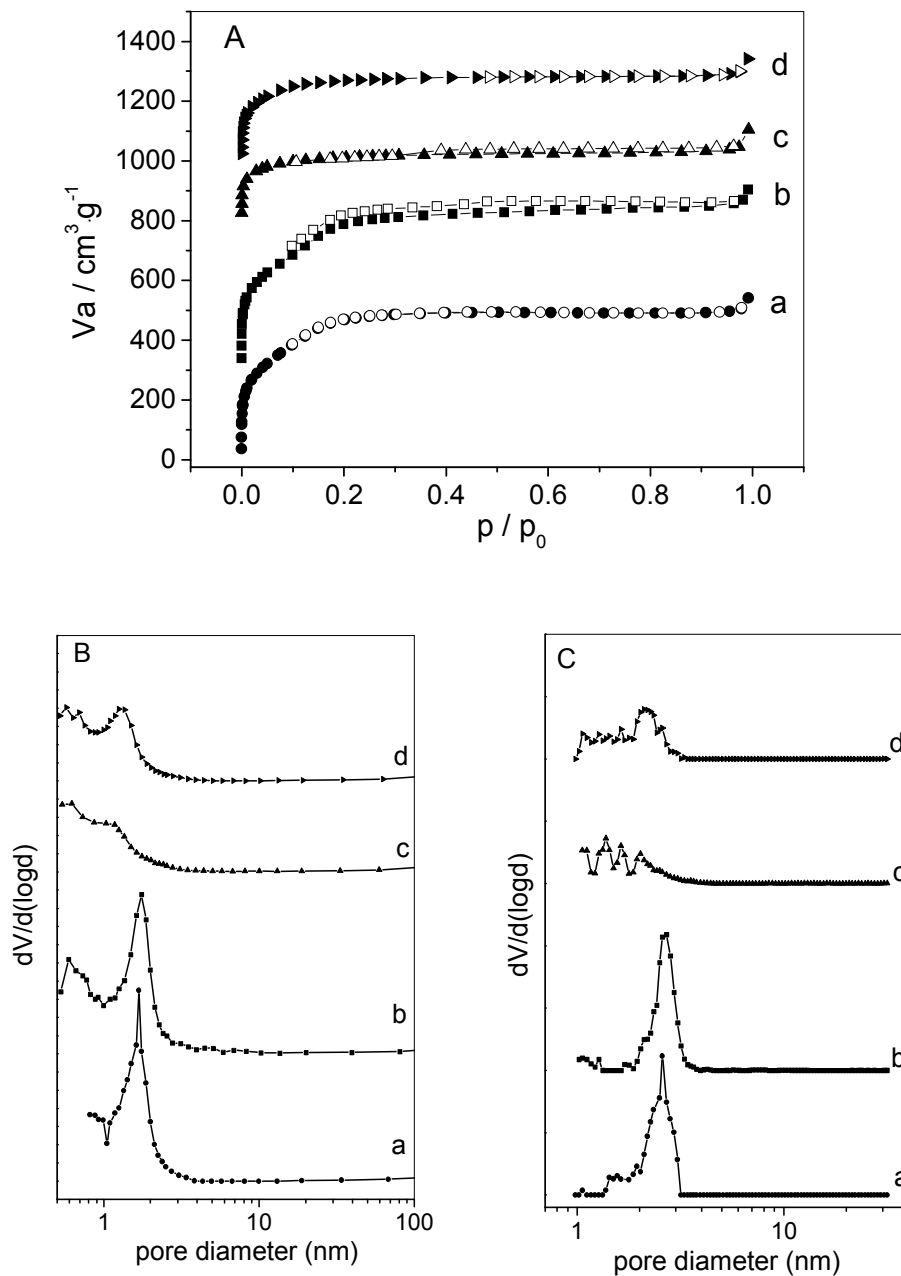


**Figure 6** N<sub>2</sub> adsorption-desorption isotherms (A) and pore size distribution calculated by BJH model (B) and NLDFT model (C) of silicas and aluminosilicates: (a) S-C<sub>12</sub>-H<sub>2</sub>SO<sub>4</sub>, (b) C<sub>12</sub>-AS-50, (c) S-C<sub>10</sub>-H<sub>2</sub>SO<sub>4</sub> and (d) C<sub>10</sub>-AS-50.

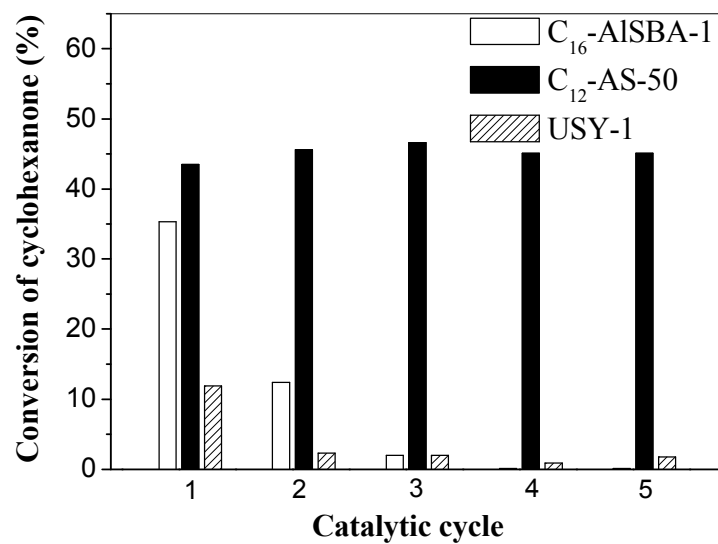
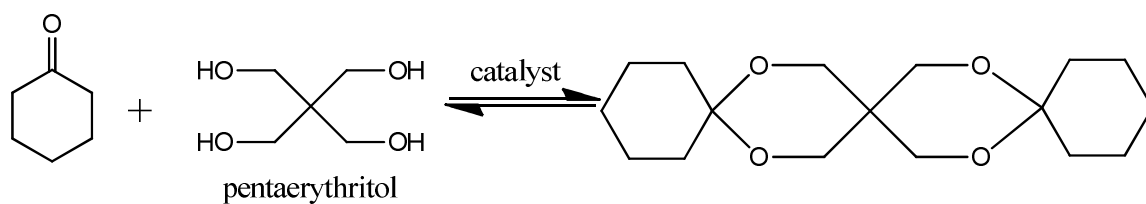
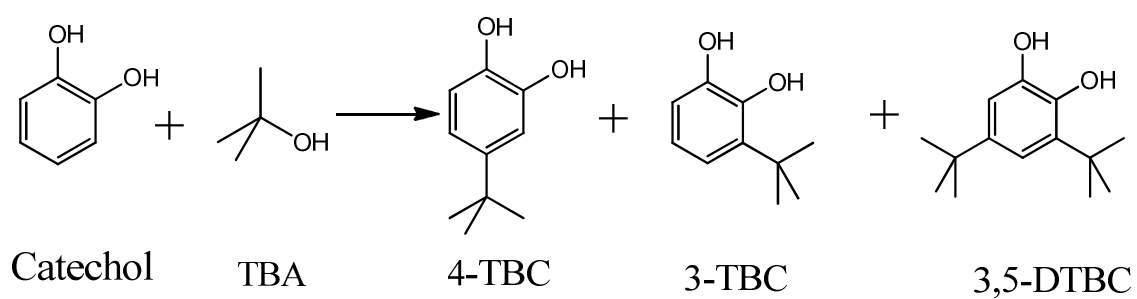


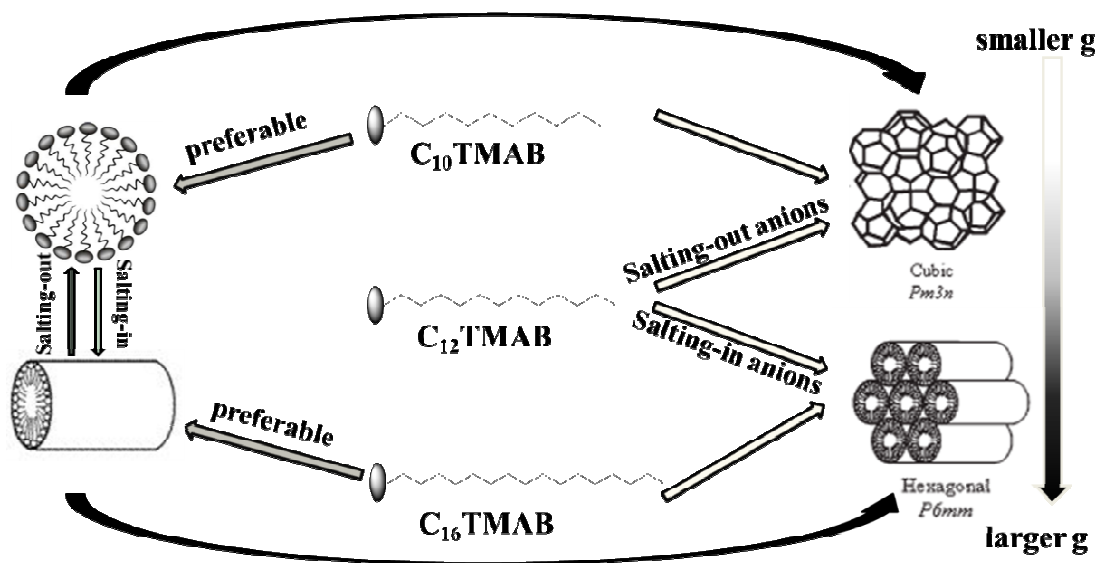
**Figure 7** Recyclability studies of the various catalysts in the acetalization of cyclohexanone with pentaerythritol.



**Scheme 1A** Acetalization of cyclohexanone with pentaerythritol.



**Scheme 1B** Illustration of alkylation of catechol with *tert*-butyl alcohol.



**Scheme 2** Illustration of the forming of cubic  $Pm3n$  and hexagonal  $p6mm$  structures templated by alkyltrimethylammonium bromide surfactants.

**Table 1** Textural properties of silicas and aluminosilicates templated by C<sub>12</sub>TMAB and C<sub>10</sub>TMAB.

samples	SiO <sub>2</sub> /Al <sub>2</sub> O <sub>3</sub>		a <sub>0</sub> <sup>a</sup> (nm)	S <sub>BET</sub> (m <sup>2</sup> ·g <sup>-1</sup> )	V <sub>total</sub> (cm <sup>3</sup> ·g <sup>-1</sup> )	d <sub>BJH</sub> (nm)	d <sub>NLDFT</sub> (nm)
	gel	product					
S-C <sub>12</sub> -H <sub>2</sub> SO <sub>4</sub>	-	-	6.62	1557	0.84	1.68	2.29, 2.53
C <sub>12</sub> -AS-50	50	51	6.81	1624	0.93	1.74	2.64
S-C <sub>10</sub> -H <sub>2</sub> SO <sub>4</sub>	-	-	5.74	795	0.47	1.17	1.35, 1.63, 2.04
C <sub>10</sub> -AS-50	50	48	5.71	1045	0.53	1.30	2.10, 2.60

$$^a a_0 = \sqrt{5} \cdot d_{210}$$

**Table 2** Results of acetalization of cyclohexanone with pentaerythritol over different catalysts.

No.	catalyst	SiO <sub>2</sub> /Al <sub>2</sub> O <sub>3</sub>	Cyclohexanone conversion (%)
1	USY-1	5.6	11.9
2	C <sub>12</sub> -AS-100	104	31.7
3	C <sub>12</sub> -AS-75	74	44.3
4	C <sub>12</sub> -AS-50	51	43.5
5	C <sub>12</sub> -AS-25	25	44.3
6	C <sub>12</sub> -AS-50-HNO <sub>3</sub>	47	42.6
7	C <sub>10</sub> -AS-50	48	43.2
8	C <sub>16</sub> -AISBA-1(71)	71	31.1
9	C <sub>16</sub> -AISBA-1(56)	56	35.3

Reaction condition: 20 mmol cyclohexanone, 10 mmol pentaerythritol, temperature = 120

°C, and time = 2 h.

**Table 3** Results of *tert*-butylation of catechol over different catalysts at various reaction temperatures.

catalyst	Acidity <sup>a</sup>	T (°C)	Conv. (%)	Selectivity (%)			Yield of 4-TBC (%)
				4-TBC	3-TBC	3,5-DTBC	
USY-1	2.75	125	48.3	88.1	6.9	5.0	42.6
		150	60.1	90.6	3.7	5.8	54.4
		175	60.9	92.4	3.1	4.5	56.3
		200	51.7	92.1	3.9	3.9	47.6
		225	29.5	93.7	4.1	2.2	27.6
C <sub>12</sub> -AS-50	0.30	125	53.1	67.1	11.3	21.6	35.6
		150	63.4	74.4	5.2	20.4	47.2
		175	74.3	85.6	3.7	10.8	63.6
		200	63.8	88.5	4.9	6.6	56.4
		225	34.8	92.6	5.7	1.7	32.2
C <sub>12</sub> -AS-50-HNO <sub>3</sub>	0.35	125	59.1	64.6	11.4	23.9	38.2
		150	65.2	72.1	7.8	20.1	47.0
		175	64.7	82.3	7.1	10.6	53.2
		200	50.1	85.5	7.8	6.6	42.8
		225	34.4	92.5	6.0	1.5	31.8
C <sub>16</sub> -AISBA-1(56)	0.28	125	42.9	67.1	12.5	20.4	28.8
		150	64.1	77.9	7.5	14.6	49.9
		175	58.4	84.3	7.1	8.6	49.2
		200	51.1	85.7	7.6	6.7	43.8
		225	32.3	89.0	7.0	3.9	28.7

Reaction conditions: catalyst = 100 mg, WHSV  $\approx$  11.0 h<sup>-1</sup>, TOS = 1 h.

<sup>a</sup> mmol NH<sub>3</sub>/g catalyst, measured by NH<sub>3</sub>-TPD.